Quality Assessment of the Wide-Angle Detection Option Planned at the High-Intensity / Extended Q-Range SANS Diffractometer KWS-2 Combining Experiments and McStas Simulations.

Aurel Radulescu[a]

[a] Jülich Centre for Neutron Science at Heinz Maier-Leibnitz Zentrum (MLZ), Forschungszentrum Jülich GmbH, Lichtenbergstr. 1, Garching, 85747, Germany

Synopsis The performance of the WANS option on pinhole SANS instruments to measure data over a wide angular range with variable resolution can be assessed by comparison with the McStas simulation of ideal experimental conditions on the instrument.

Abstract For a reliable characterization of materials and systems featuring multiple structural levels, a broad length scale from a few Å to hundreds of nm must be analyzed and an extended Q range must be covered in the X-ray and neutron scattering experiments. For special samples or effects, it is advantageous to perform such characterization with a single instrument. Neutrons offer the unique advantage of contrast variation and matching by D-labeling, which is of great value in the characterization of natural or synthetic polymers. Some TOF-SANS instruments at neutron spallation sources can cover an extended *Q*-range by using a broad wavelength band and a multitude of detectors arranged to cover a wide range of scattering angles with a resolution that allows both large-scale morphology and crystalline structure to be resolved simultaneously. However, for such analyses, the SANS instruments at steady-state sources operating in conventional monochromatic pinhole mode should rely on additional WANS detectors and tune the resolution via a system of choppers and a TOF data acquisition option to reliably measure the atomic to mesoscale structures. The KWS-2 SANS diffractometer allows the exploration of a wide *Q*-range using conventional pinhole and lens focusing modes and an adjustable resolution $\Delta\lambda/\lambda$ between 2% and 20% through the use of a versatile mechanical velocity selector combined with a variable slit opening and rotation frequency chopper. The installation of WANS detectors planned on the instrument required a detailed analysis of the quality of the data measured over a wide angular range with variable resolution, so that an assessment of the WANS performance can be achieved by comparison with the McStas simulation of ideal experimental conditions at the instrument.

Keywords: SANS; WANS; McStas simulation; semi-crystalline materials

1. Introduction

Materials based on semi-crystalline polymers exhibit a phase separation in crystalline and amorphous regions, and are characterized by a complex morphology with hierarchically organized multiple structural levels that spans a wide length scale between several Å and hundreds of micrometers (Akpalu, 2010; Radulescu et al., 2015a; Kanaya et al., 2007). Moreover, the bulk and interlamellar amorphous regions can be functionalized, that results in even more complex morphologies when external stimuli such as humidity, temperature or elongation / compression are applied to the sample (Schiavone et al., 2023). For the characterization of such complex morphologies, a wide length scale has to be covered, which usually requires a combination of different experimental methods in the structural analysis. Combination of wide- and small-angle techniques with X-rays (WAXS and SAXS) have long been used in such experimental investigations (Kanaya, et al., 2007; Koga et al., 2008; Hama & Tashiro 2003; Schneider, 2010). SAXS provides information about the overall morphology of polymers and their higher order structural levels, while the crystalline structure of polymers can be investigated with WAXS. Similar to X-rays, neutrons are an excellent probe for characterizing such complex morphologies over a wide length scale. Additionally, neutrons offer the unique advantage of different interactions with the ^{1}H and ^{2}H (deuterium, D) hydrogen isotopes, thus the possibility to vary the scattering contrasts between different constituents of a hydrocarbon sample over a broad range by H/D substitution (Jacques & Trewhella, 2010). This makes the small-angle (SANS) and wide-angle (WANS) neutron scattering techniques particularly suitable for the detailed investigation of natural and synthetic multi-component polymeric materials. However, while modern X-ray lab diffractometers or beam lines at large scale facilities can easily and successfully combine USAXS/SAXS/WAXS (Pauw et al., 2021), in the case of neutron scattering such a combination of methods require a special care. WANS and SANS can be simultaneously performed without technical and organizational difficulties with TOF-SANS instruments at spallation sources, where a broad wavelength band is used and a wide angular range of scattering can be covered by using a large number of detectors either movable (Heenan et al., 2005; Zhao et al., 2010) or placed in fixed positions (Takata et al., 2014; Koizumi et al., 2020; Allen, 2023). In contrast, classical pinhole SANS diffractometers at steady-state neutron sources (nuclear reactors) must be combined with wide-angle neutron diffractometers to extend the Q-range to higher Q values. However, simultaneous use of wide- and small-scattering

methods in the same experiment is necessary for sensitive or expensive samples, if special care must be paid to sample preparation (composition, quality, amount, etc.) or in-situ treatment (temperature, humidity, chemical condition, etc.) during the experimental investigation (Tashiro & Sasaki, 2003). To overcome these difficulties, one should thus be able to cover an extended *Q* range at the same pinhole SANS diffractometer. Some pinhole instruments were already equipped with focusing lenses for measurements at lower *Q*-values (Koizumi et al., 2007; Wood et al., 2018; Barker et al., 2022) and with wide-angle detectors for covering higher *Q*-values (Heller et al., 2018) in an attempt to extend their *Q*-range as far as possible in both directions.

The small-angle neutron diffractometer KWS-2 (Radulescu et al., 2012a) operated by the Jülich Centre for Neutron Science (JCNS) at the Heinz Maier-Leibnitz Zentrum (MLZ), Garching, Germany, is dedicated to the investigation of mesoscopic multi-scale structures and structural changes in soft condensed matter and biophysical systems. Following demands from the user community, it was repeatedly upgraded to enable the exploration of a broad *Q* range, between 2.0 x 10^{-4} and 1.0 $Å^{-1}$, providing high neutron intensities and a tunable experimental resolution (Radulescu et al., 2015b; Houston et al., 2018). The broad *Q* range is currently covered by combining in a versatile user-friendly approach the conventional pinhole and focusing working modes. In the conventional pinhole mode, the wavelength λ and the sample to main detector distance L_D can be varied between 2.8 and 20 Å and from 1.25 m to 20 m, respectively, to maximize the *Q*-range. The main detection system of KWS-2 consists of an array of ^{3}He tubes and rapid read-out electronics (Houston et al., 2018). In focusing mode parabolic MgF_2 lenses are used in combination with a small aperture at the entrance of the collimation system and a secondary scintillation-type high-resolution detector (HRD) that can be automatically be brought in beam on demand (Radulescu et al., 2012a).

With the ultimate goal of providing KWS-2 with diffraction capabilities that bridge from atomic- to meso-scale structures, a new upgrade of the instrument is currently underway, aiming to combine short wavelengths (λ = 2.8 Å) with wide-angle detection of scattered neutrons up to a scattering angle θ_s = 50° to achieve a Q_{max} = 2.0 $Å^{-1}$. This allows a broad *Q* range between 2 x 10^{-4} and 2.0 $Å^{-1}$ to be covered, enabling full structural characterization of the sample of interest using only one instrument and one sample geometry. The current

upgrade will then allow WANS and SANS measurements on KWS-2 in different combinations of standard and TOF modes with adjustable resolution for different scientific objectives: observation of crystalline peaks or form factor details of small size morphologies, minimization of incoherent background, etc. Recent studies (Schiavone et al., 2023; Hirai et al., 2019) have shown the tremendous gain in structural characterization of multicomponent systems characterized by different structural levels while investigating both the meso and short length scales in one experiment when a broad *Q* range can be covered in a combined SANS-WANS experimental approach at the same instrument. In addition, the WANS detectors at KWS-2 will enable suitable TOF conditions to gain insight into the inelastic scattering of hydrogenated samples (Balacescu et al., 2021) and reduce the incoherent background, which is useful when data collected at high *Q* do not show a flat profile.

The two future detection systems at KWS-2, the SANS and WANS detectors, will operate independently, with the collimation, resolution and TOF conditions properly set for defined scientific purposes. The data quality of the main SANS detector has been characterized in detail in a previous work (Houston et al., 2018). The results of recent tests on KWS-2 to assess the quality of the measured data with adjustable resolution at different scattering angles covering a wide angular range beyond that of the conventional SANS setup are reported here in comparison with the results of McStas simulations of the virtual ideal experimental setup.

2. Experimental

In this study, the reflection from the crystalline planes (111) of fullerene-C60 was followed for the assessment of the data quality measured at KWS-2 in TOF mode in the SANS and WANS regimes, respectively. Fullerene-C60 powder from Sigma-Aldrich (Germany) was first structurally characterized by XRD in the range of θ_s between 5° and 60° with an X-ray powder diffractometer Bruker 2nd Gen-D2 Phaser (Cu-source), then prepared in Hellma banjo-type quartz cuvette for the SANS investigation at the pinhole SANS diffractometer KWS-2 (Radulescu et al., 2015b; Houston et al., 2018). XRD characterization of a silver behenate (AgBeh) powder sample (AlfaAesar, Germany) was carried out in parallel.

SANS was performed in the high-*Q* regime using the main detector at L_D = 1.25 m for two experimental setups: (i) with a wavelength λ = 3.0 Å as provided by a 36-blade velocity selector (Airbus, Germany) used in a tilted position in the beam (tilt angle ξ = -10°) for a wavelength resolution of $\Delta\lambda/\lambda$ = 22.7 % (Houston et al, 2018), and (ii) with a wavelength λ = 2.8 Å with $\Delta\lambda/\lambda$ = 4.7 % in TOF mode with the resolution chopper (Radulescu et al. , 2015b) used together with the tilted 72-blade velocity selector (Airbus, Germany) in a tilted position in the beam (ξ = -10°). One should bear in mind that the two velocity selectors provide a nominal full wavelength distribution $\Delta\lambda/\lambda$ of 20.6 % and 10.9 %, respectively, when they are used in the standard configuration (λ_{min} = 4.5 Å), parallel to the beam axis, and of 22.7 % (λ_{min} = 3.0 Å) and 14 % (λ_{min} = 2.8 Å), respectively, when they are used in tilted position at the maximum rotation speed (Radulescu et al., 2023; Houston et al., 2018). The weaker worsening of wavelength resolution in inclined configuration for these short wavelengths compared to $\lambda \geq$ 4.5 Å (35.3% and 18.5%, respectively, as reported by Houston et al., 2018, and Radulescu et al., 2023) is due to the effect induced by the neutron guide cut-off of the KWS-2 instrument (Radulescu et al., 2012b, Houston et al., 2018). The cut-off of a neutron guide refers to the rapid drop in brightness at lower wavelengths caused by the upstream guide's curvature combined with the wavelength dependence of the critical angle of reflection from the mirror coating of the guide. The guide cut-off is also responsible for the slightly different λ_{min} obtained when the two selectors are used at maximum rotation speed in tilted configuration. The opening of the rectangular source aperture, which was located in front of the sample at a collimation length of L_C = 4 m, was 50 mm x 50 mm, while the opening of the sample aperture was 10 mm x 10 mm. The data were collected on the main detector of the instrument, which consists of an array of ^{3}He tubes with a pixel size of 8 mm x 8 mm.

WANS test investigation was carried out on fullerene-C60 sample with a portable scintillation HRD installed at the sample position, immediately after the sample (L_D = 30 cm), at an angle of 30° between the detector axis and the beam axis. The active area of the HRD is characterized by a diameter of 9 cm and a pixel size is 0.4 mm x 0.4 mm. Data were collected with λ = 5 Å, delivered by the tilted velocity selector) for a $\Delta\lambda/\lambda$ = 6.2% as obtained by collecting data in TOF mode using the resolution chopper in concert with the velocity selector (Radulescu et al., 2015b).

Typical corrections for the empty cuvette contribution, dark current and detector sensitivity determined with a slab of Plexiglas secondary standard (Houston et al, 2018) were applied to the raw-data, which were subsequently calibrated in absolute units using the Plexiglas secondary standard (Houston et al., 2018) and radially averaged over the entire detection area, while the WANS data were averaged only on a narrow equatorial sector of the HRD.

3. Simulations

Data measured on fullerene-C60 were compared with the results of simulations of the ideal experimental conditions, including neutron source, guide system, selector, collimator, sample and detector, using the McStas program package (Willendrup, et al., 2004). The KWS-2 instrument option for McStas, including different velocity selector states, was used in previous simulations as reported by Radulescu et al. (2008, 2012b). For the currently reported simulation the McStas component Powder1.comp was used to describe the fullerene-C60 powder sample, based on the scattering pattern observed by XRD (Sanz et al., 2015).

4. Results and Comments

AgBeh is a wavelength calibrant used in small-angle scattering experiments with X-rays (SAXS) and neutrons (SANS), as reported by Ilavsky et al. (2018) and Houston et al. (2018). The Bragg spacing of AgBeh is known to be d_{AgBeh} = 58.38 Å (Okabe et al., 2007). However, the crystalline scattering pattern of AgBeh in the wide-angle scattering regime, up to Q_{max} = 2.0 $Å^{-1}$, is characterised by a large number of peaks (Tan et al., 2020), that make difficult to use this system for the purpose of calibration in wide-angle measurement geometry. Ilavski et al. (2018) reported the availability of different NIST X-ray powder diffraction calibration standards for the wide-angle scattering regime, such as SRM 640 based on silicon and SRM 660 based on lanthanum hexaboride LaB_6, which are considered for calibration of the WANS setup at the USAXS/SAXS/WAXS beamline of the Advance Photon Source (APS), Argonne National Laboratory, USA.

In contrast to AgBeh, fullerene C60 is characterized by isolated and very sharp crystalline reflections in the *Q* range corresponding to wide-angle scattering. The reflection from the crystalline planes (111) appears at θ_s = 10.78° in XRD patterns obtained with Cu-Kα source

(Sathish & Miyazawa, 2010). In Q-range this crystalline reflection will appear isolated at Q_{C60} = 0.766 Å^{-1} (Sanz, et al., 2015). Fig. 1 shows the XRD results from the fullerenes-C60 sample in parallel to those measured on AgBeh. The suitability of using the fullerene-C60 powder sample as a model system and observe the 111 reflection for the purpose of assessing the data quality measured in the WANS regime is evident from this parallel. In a SANS experiment, this reflection will be observed as a ring appearing at the scattering angles of θ_s = 19.68° when neutrons with λ = 2.8 Å will be used, while with neutrons with λ = 5.0 Å and 7.0 Å the peak will be observed in the WANS regime at θ_s = 35.53° and 50.57°, respectively.

Fig. 2 shows the splitting scheme of the trapezoidal wavelength distribution acquired in TOF mode for a pulse delivered by the chopper when measuring 111 reflection from the fullerene C60 powder sample when a wavelength delivered by the velocity selector λ = 2.8 Å was used, and the scattering patterns corresponding to each time channel as recorded on the main ^{3}He detector. The double-disc resolution chopper pulsed the beam and transformed the triangular distribution delivered by the velocity selector with $\Delta\lambda/\lambda$ = 14% into a trapezoidal one, due to the opening time of the chopper window, τ_w. This is due to the fact that the KWS-2 double disk chopper can practically be considered as a single disk chopper, since the two disks rotate at the same speed (Radulescu et al., 2015b). In this case, the TOF resolution is determined by τ_w, which depends on the chopper frequency $f_{chopper}$ and the angular opening of the window $\Delta\varphi$, which can be adjusted by suitable positioning of the two disks relative to each other. Technical details and setting parameters of the KWS-2 chopper can be found in Radulescu et al. 2015b. In the simple TOF mode with the KWS-2 chopper, one aims to divide the wavelength band into n equal parts (as shown schematically in Fig. 2). In principle, τ_w is set so that it corresponds to the n^{th} part of the wavelength band. For the SANS measurement of the fullerene-C60 powder sample $f_{chopper}$ and $\Delta\varphi$ were set to deliver TOF channels with a width of τ_w = 0.00072 s, which allowed the trapezoidal pulse delivered by the selector/chopper tandem to be split into seven TOF channels. Thus, the width of the central TOF channel corresponded to $\Delta\lambda/\lambda$ = 4.7 %. The TOF-distance plots and examples of different experimental setups to achieve the desired resolution in the TOF channels of the split wavelength distribution are described in detail in Radulescu et al. (2015b).

The 2D scattering pattern corresponding to each TOF channel displays the narrow ring like scattering feature from the 111 reflection of the powder sample. The position of the ring scattering feature on the 2D detector changes from channel to channel due to different wavelength corresponding to each channel, which makes the scattering from the same structural feature to appear at a different scattering angle (Radulescu et al., 2015b).

Fig. 3 presents a parallel of the 2D SANS patterns from the fullerenes-C60 sample as delivered by measurements with and without chopper used and the McStas simulations for the same conditions, namely λ = 3.0 Å with $\Delta\lambda/\lambda$ = 22.7% for only the velocity selector considered (panels a and c) and λ = 2.8 Å with $\Delta\lambda/\lambda$ = 4.7% (panels b and d), respectively. A broad ring-like scattering feature representing the 111 reflection from the fullerene-C60 powder sample can be observed towards the rim of the detector in both experimental and simulated cases for the conventional measurement mode while, as a consequence of a better wavelength resolution, a very narrow width ring like scattering feature is observed in both measured and simulated scattering patterns when the chopper is used in concert with the velocity selector and the data are sorted out in TOF mode. Fig. 3b presents the scattering pattern corresponding only to the central TOF channel (the 4th TOF channel in the trapezoidal distribution shown in Fig. 2), characterized by λ = 2.8 Å and $\Delta\lambda/\lambda$ = 4.7%. The large width of the scattering feature measured in conventional mode is due to the large $\Delta\lambda/\lambda$ used in this experiment, while the asymmetric aspect of the scattering pattern with respect to the detector geometry is due to the off-centered positioning of the detector in beam. Although this is outside the scope of the present study and no additional analysis was performed here, it can only be speculated that the fringe features observed along the azimuthal and radial directions in Fig. 3a could be an effect of the granular powder character of the sample (Kaduk et al., 2021), which was investigated under the broad $\Delta\lambda/\lambda$ measurement conditions.

The scattering results from the 111 reflection of the fullerene-C60 powder sample collected in TOF mode with the portable HRD installed at the sample position in WANS geometry are shown in Fig. 4a, again from only the central TOF channel of the wide trapezoidal distribution provided by the velocity selector/chopper tandem. The experiment was carried out with a neutron wavelength λ = 5 Å, as delivered by the velocity selector at a wavelength spread of $\Delta\lambda/\lambda$ = 18.5%. The chopper settings were adjusted to provide a central TOF

channel width corresponding to $\Delta\lambda/\lambda$ = 6.2%, which allowed to split the pulse delivered by the selector/chopper tandem into seven TOF channels, similarly to scheme shown in Fig. 2. Fig. 4b and 4c show the simulated results for the same experimental conditions as a function of x,y position on the 2D detector and of scattering angle using the PSD_monitor and Div1D_monitor McStas components, respectively. Arcs of high intensity were observed on the HRD representing a portion of the ring like scattering feature due to the 111 reflection from the powder sample. For these experimental conditions the 111 reflection is observed at θ_s = 35.53°, out of the center of the HRD, that corresponds to an angle of θ_s = 30°.

The measurement of the 111 crystalline reflection of fullerene-C60 using the combination of SANS and WANS with different instrumental resolutions demonstrates the good quality of such results when also compared the radially averaged 1D neutron scattering patterns to the XRD data (green line in Fig. 5). Moreover, the measured and simulated WANS signal from fullerene-C60 powder sample (black empty symbols and yellow curve in Fig. 5) are coinciding quite well for the same experimental conditions considered. This approach also proves that SANS and WANS measurements may be simultaneously carried out at a pinhole SANS diffractometer provided that the right resolution for different scientific goals (sharp crystalline peaks, form factor details, incoherent background determination, etc.) may be selected in a versatile way and the instrument is equipped with wide angle detectors that can operate in a fixed position simultaneously with the movable main detector, with a proper adjustment of collimation system. Also, both kinds of detectors should be able to collect data in TOF or continuous modes, depending on the scientific goals of the experiment. All this versatility is currently available at KWS-2, with the wavelength resolution tunable between 2% and 20% (Radulescu et al. 2015; Radulescu et al, 2023), reaching thus the required resolution for resolving crystalline peaks, comparable to that of TOF-SANS instruments at spallation sources (Schiavone et al., 2023). Based on the current quality assessment of the WANS data, the WANS detectors (2D-3He tube arrays as reported by Radulescu et al.; 2023) are currently in the purchasing phase and the WANS option is in the planning phase at KWS-2. Finally, one should mention that in the Q-range between 1 $Å^{-1}$ and 2 $Å^{-1}$ the instrumental resolution is depending on $\Delta\lambda/\lambda$ with no observable effect from the collimation contribution (Fig. 6), that opens the possibility to improve the intensity on

the sample by working with a short collimation L_C = 4m or 2m in the intensity unfavorable TOF mode, without a deterioration of the quality of the scattering features.

In conclusion, combining the analysis of the experimental data collected with tunable instrumental resolution over a wide angular range, beyond the limits of the conventional SANS setup, with the McStas simulation results it was demonstrated that the proposed WANS setup for KWS-2 instrument will be suitable for measurement of fine scattering details up to θ_s = 50°. This will enable the targeted Q_{max} and the possibility to improve the signal-to-noise ratio by separating the inelastic scattering from the elastic scattering in TOF when data at high Q do not show a flat profile, for which a flight path of L_D > 1m is needed, as shown by Balacescu et al., 2021.

Acknowledgements The help from Dr. Ralf Engels and Dr. Georg Brandl, both from Forschungszentrum Jülich, during the WANS test with the HRD at KWS-2 is kindly acknowledged.

References

Akpalu, Y. V. (2010). Polym. Rev. 50, 1–13.

Allen, A. J. (2023) J. Appl. Cryst. 56, 787-800.

Balacescu, L; Brabdl, G. & Radulescu, A. (2021) J. Appl. Cryst. 54, 1217-1224.

Barker, J.; Moyer, J.; Kline, S.; Jensen, G.; Cook, J.; Gagnon, C.; Kelley, E.; Chabot, J.P.; Maliszewskyj, N.; Parikh, C.; Chen, W.; Murphy, R. P. & Glinka, C. (2022) J. Appl. Cryst. 55, 271-283.

Hama, H. & Tashiro, K. (2003) Polymer 44, 2159-2168.

Heenan, R. K.; King, S. M.; Turner, D. S. & Treadgold, J. R. (2005) Proc. ICANS – XVII, 780–785.

Heller, W. T.; Cuneo, M.; Debeer-Schmitt, L.; Do, C.; He, L.; Heroux, L.; Littrell, K.; Pingali, S. V.; Qian, S.; Stanley, C.; Urban, V. S.; Wu, B. & Bras, W. (2018) J. Appl. Cryst. 51, 242-248.

Hirai, M.; Ajito, S.; Arai, S.; Adachi, M.; Shimizu, R.; Wakamatsu, K.; Takata, S. & Iwase, H. (2019) J. Phys. Chem. B 123, 3189-3198.

Houston, J. E.; Brandl, G.; Drochner, M.; Kemmerling, G.; Engles, R.; Papagiannopoulos, A.; Sarter, M.; Stadler, A. & Radulescu, A. (2018) J. Appl. Cryst. 51, 323-336.

Ilavsky, J.; Zhang, F.; Andrews, R. N.; Kuzmenko, I.; Jemian, P. R.; Levine, L. E. & Allen, J. (2018) J. Appl. Cryst. 51, 867-882.

Jacques, D. A. & Trewhella, J. (2010) Protein Science 19, 642-657.

Kaduk, J. A.; Billinge, S. J. L.; Dinnebier, R. E.; Henderson, N.; Madsen, I.; Cernys, R.; Leoni, M.; Thakral, S. & Chateigner, D. (2021) Nat. Rev. Methods Primers 1, 77.

Kanaya, T.; Matsuba, G.; Ogino, Y.; Nishida, K.; Shimizu, H. M.; Shinohara, T.; Oku, T.; Suzuki, J. & Otomo, T. (2007) Macromolecules 40, 3650-3654.

Koga, T.; Hashimoto, T.; Takenaka, M.; Aizawa, K.; Amino, N.; Nakamura, M.; Yamaguchi, D. & Koizumi, S. (2008) Macromolecules 41, 453-464.

Koizumi, S.; Iwase, H.; Suzuki, S.; Oku, T.; Motokawa, R.; Sasao, H.; Tanaka, H.; Yamaguchi, D.; Shimizu, H. M. & Hashimoto, T. (2007) 40, s474-s479.

Koizumi, S.; Noda, Y.; Maeda, T.; Inada, T.; Ueda, S.; Fujisawa, T.; Izunome, H.; Robinson, R. A. & Frielinghaus, H. (2020) QuBS 4, 42.

Okabe, S.; Karino, T.; Nagao, M.; Watanabe, S. & Shibayama, M. (2007) Nucl. Instrum. Methods Phys. Res. Sect. A 572, 853–858.

Pauw, B. R.; Smith, A. J.; Snow, T.; Shebanova, O.; Sutter, J. P.; Ilavsky, J.; Hermida-Merino, D.; Smales, G. N.; Terrill, N. J.; Thuenemann, A. F. & Bras, W. (2021) J. Synchrotron Rad. 28, 1-10.

Radulescu, A.; Fetters, L. J. & Richter, D. (2008a) Adv. Pol. Sci. 210, 1-100.

Radulescu, A. & Ioffe, A. (2008b) Nucl. Instrum. Methods Phys. Res. Sect. A 586, 55-58.

Radulescu, A., Pipich, V., Frielinghaus, H. & Appavou, M. S. (2012a). J. Phys. Conf. Ser. 351, 012026.

Radulescu, A., Pipich, V. & Ioffe, A. (2012b) Nucl. Instrum. Methods Phys. Res. Sect. A, 689, 1–6.

Radulescu; A., Goerigk; G., Fetters; L. & Richter, D. (2015a) J. Appl. Cryst. 48, 1860–1869.

Radulescu, A., Szekely, N., Polachowski, S., Leyendecker, M., Amann, M., Buitenhuis, J., Drochner, M., Engels, R., Hanslik, R., Kemmerling, G., Lindner, P., Papagiannopoulos, A., Pipich, V., Willner, L., Frielinghaus, H. & Richter, D. (2015b) J. Appl. Cryst. 48, 1849-1859.

Radulescu, A.; Kang, J-J.; Appavou, M-S. & Papagiannopoulos, A. (2023) EPJ Web of Conferences 286, 03006.

Sanz, A., Wong, H. C., Nedoma, A. J., Douglas, J. F. & Cabral, J. T. (2015) Polymer, 68, 47-56.

Sathish, M. & Miyazawa, K. (2010) Cryst. Eng. Comm. 12, 4146-4151.

Schiavone, M-M.; Lamparelli, D.H.; Daniel, C.; Golla, M.; Zhao, Y.; Iwase, H.; Arima-Osonoi, H.; Takata, S.; Szentmiklosi, L.; Maroti, B.; Allgaier, J. & Radulescu, A. (2023) J. Appl. Cryst. 56, 947-960.

Schneider, K. (2010) J. Pol. Sci. B: Pol. Phys. 48, 1574-1586.

Takata, S.; Suzuki, J.; Shinohara, T.; Oku, T.; Tominaga, T.; Ohishi, K.; Iwase, H.; Nakatani, T.; Inamura, Y.; Ito, T.; Suzuya, K.; Aizawa, K.; Arai, M.; Otomo, T. & Sugiyama, M. (2014) JPS Conf. Proc. 8, 036020.

Tan, W. L.; Cheng, Y.-B. & McNeill, C.R. (2020) J. Mater. Chem. A. 8, 12790-12798.

Tashiro, K. & Sasaki, S. (2003) Polymer 28, 451-519.

Willendrup, P.; Farhi, E. & Lefmann, K. (2004). Physica B, 350, E735–E737.

Wood, K.; Mata, J. P.; Garvey, C. J.; Wu, C.-M.; Hamilton, W. A.; Abbeywick, P.; Bartlett, D.; Bartsch, F.; Baxter, P.; Booth, N.; Brown, W.; Christoforidis, J.; Clowes, D.; d'Adam, T.; Darmann, F.; Deura, M.; Harrison, S.; Hauser, N.; Horton, G.; Federici, D.; Franceschini, F.; Hanson, P.; Imamovic, E.; Imperia, P.; Jones, M.; Kennedy, S.; Kim, S.; Lam, T.; Lee, W. T.; Lesha, K.; Mannicke, D.; Noakes, T.; Olsen, S. R.; Osborn, J. C.; Penny, D.; Perry, M.; Pullen, S. A.; Robinson, R. A.; Schulz, J. C.; Xiong, N. & Gilbert, E. P. (2018) J. Appl. Cryst. 51, 294–314.
Zhao, J. K.; Gao, C. Y. & Liu, D. (2010) J. Appl. Cryst. 43, 1068–1077.

Figures

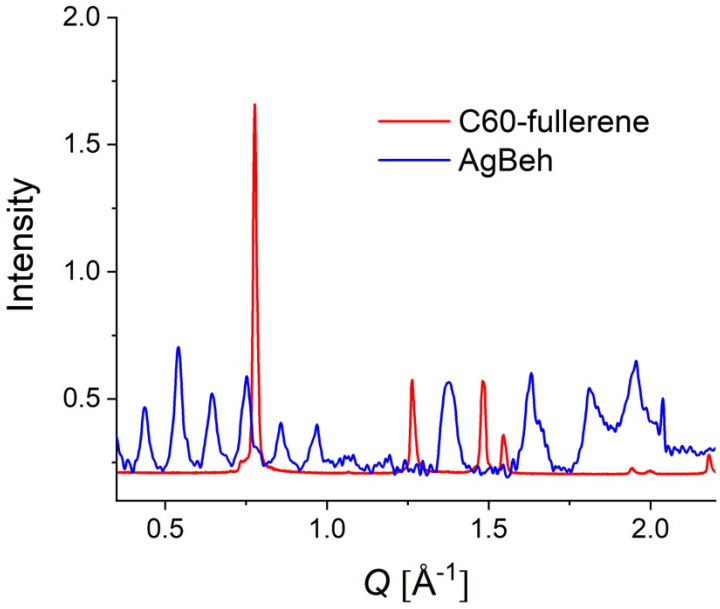

Figure 1 Scattering patterns from silver behenate (AgBeh) and C60-fullerenes obtained by XRD.

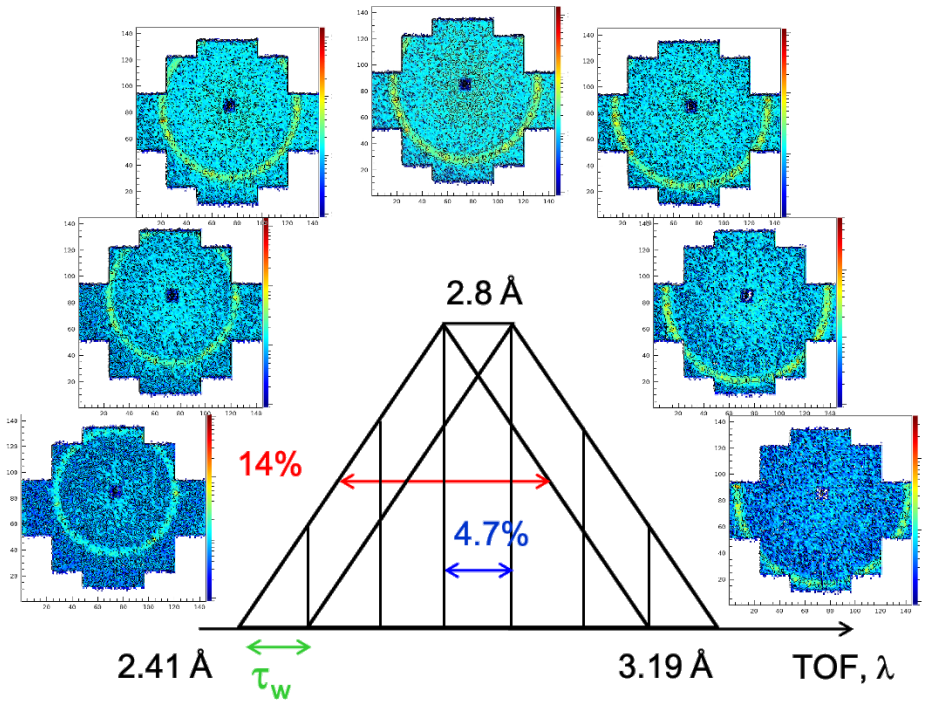

Figure 2 Scattering patterns from fullerene-C60 powder sample obtained by TOF SANS at KWS-2 for the following experimental conditions: λ = 2.8 Å and $\Delta\lambda/\lambda$ = 14%, as delivered by the tilted velocity selector, L_D = 1.25 m, $f_{chopper}$ = 98.24 Hz, $\Delta\varphi$ = 25.72°, τ_w = 0.00072 s, $\Delta\lambda/\lambda_{aim}$ = 4.7% (central TOF channel), n_{chan} = 7.

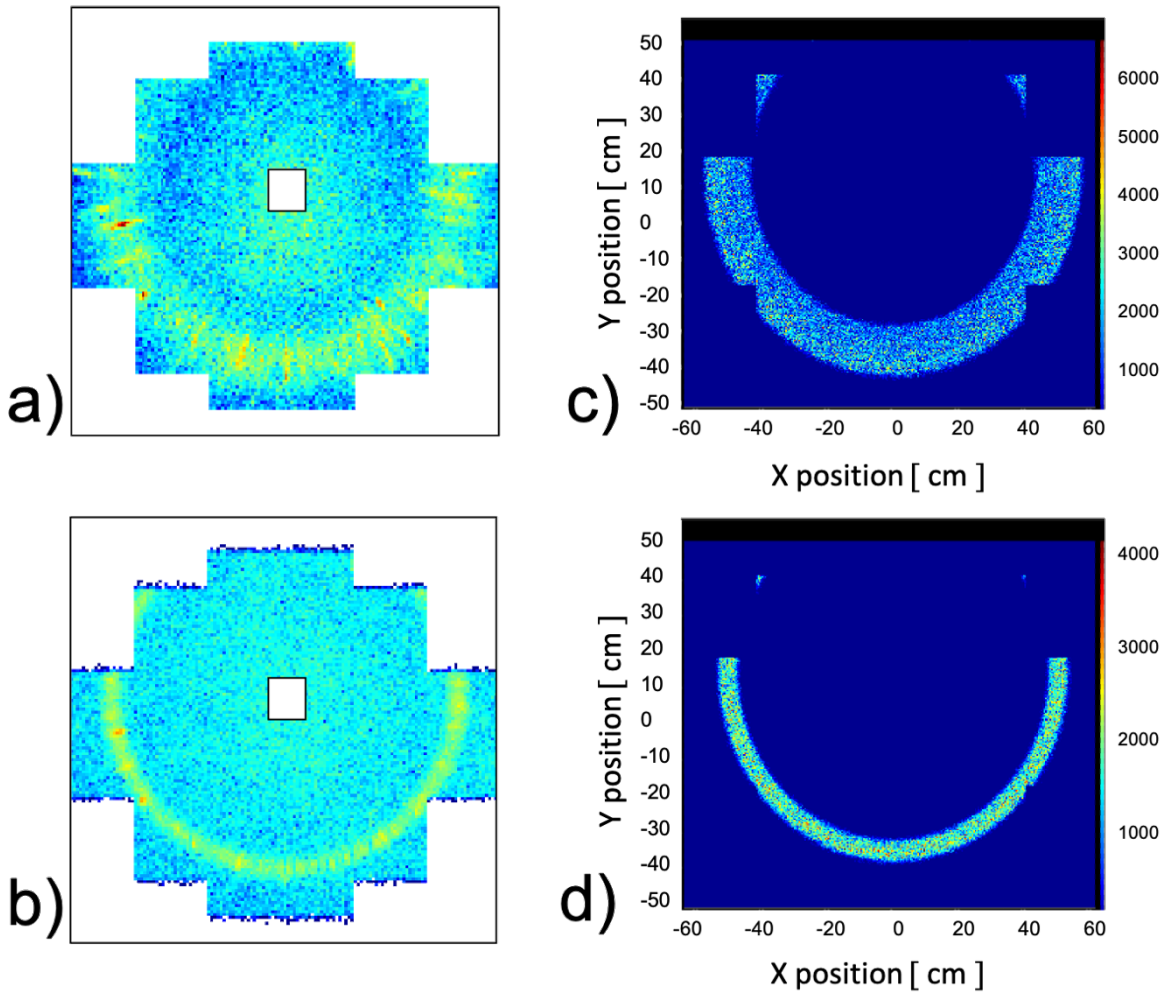

Figure 3 Measured (a, b) and simulated (c, d) two-dimensional scattering pattern from the fullerene-C60 powder sample for $\lambda = 3.0$ Å and $\Delta\lambda/\lambda = 22.7\%$ (a, c) and $\lambda = 2.8$ Å and $\Delta\lambda/\lambda = 4.7\%$ (b, d), respectively.

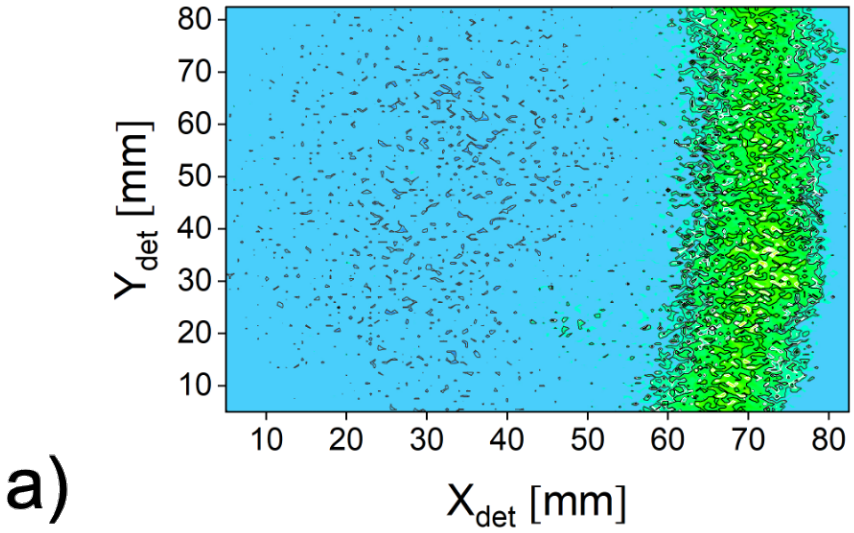
a)
Y_{det} [mm]
X_{det} [mm]
10
20
30
40
50
60
70
80

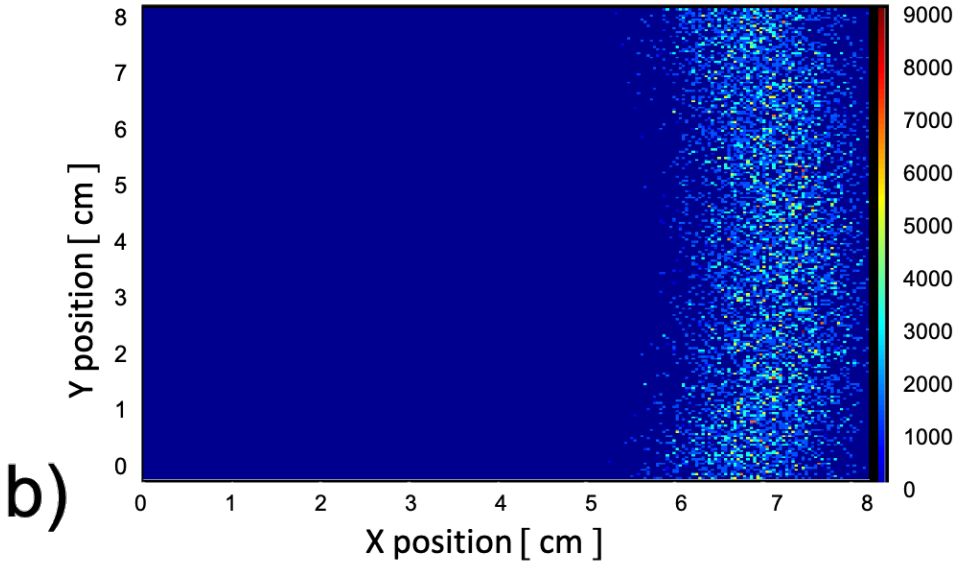
b)
Y position [cm]
X position [cm]
0
1
2
3
4
5
6
7
8
9000
8000
7000
6000
5000
4000
3000
2000
1000

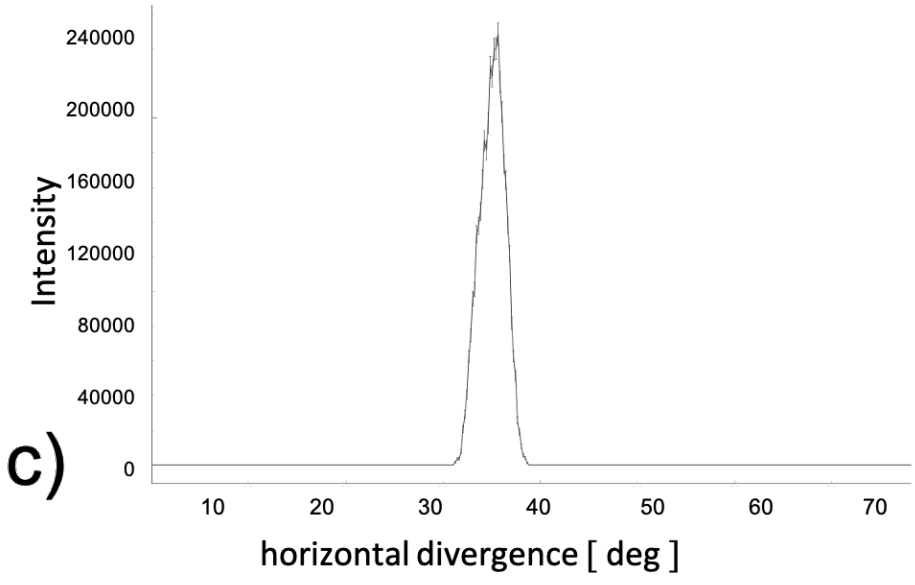
c)
Intensity
horizontal divergence [deg]
0
40000
80000
120000
160000
200000
240000
10
20
30
40
50
60
70

Figure 4 Measured with a HRD (a) and simulated (b) two-dimensional scattering pattern from the fullerene-C60 powder sample for λ = 5.0 Å and Δλ/λ = 6.2%; the HRD was used in the TOF-WANS mode (see text); panel c) shows the simulated data as a function of the scattering angle using the Div1D_monitor McStas component.

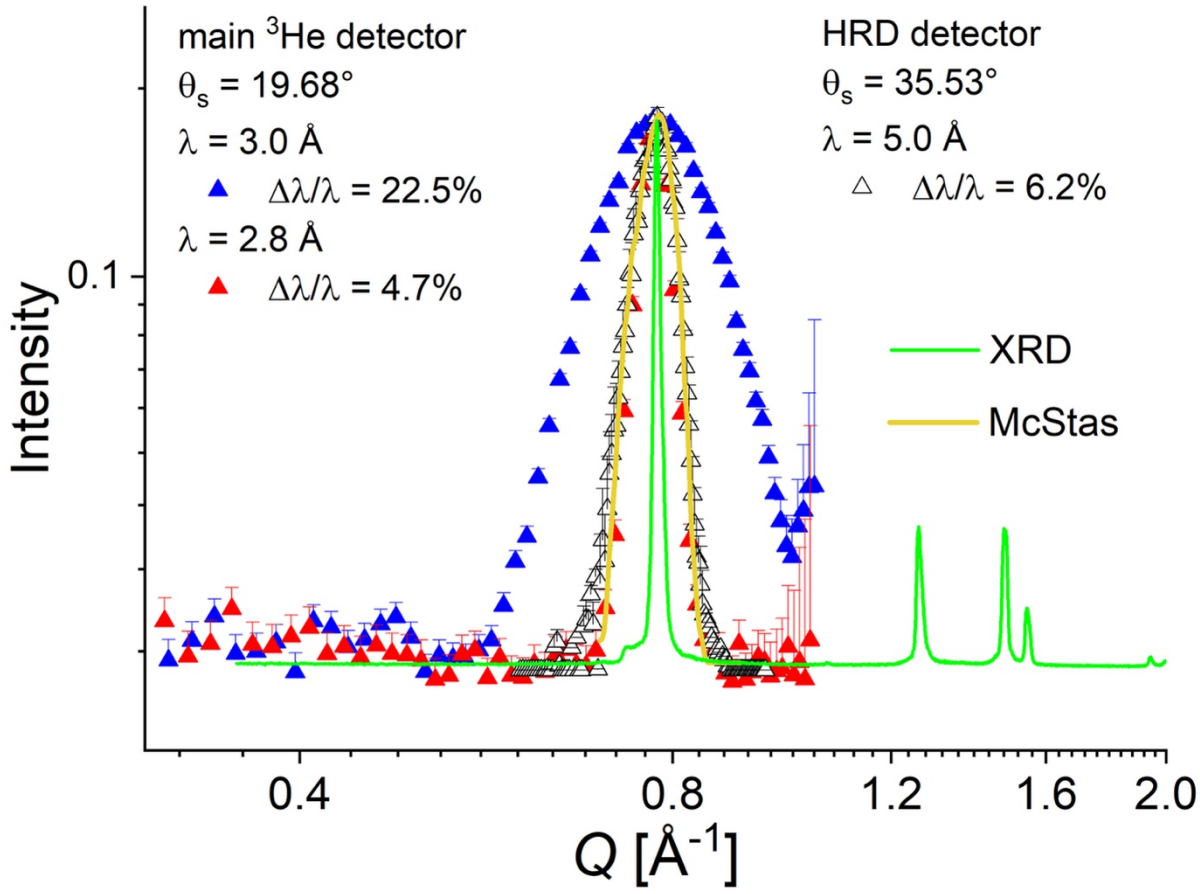

Figure 5 Measured (symbols) and simulated (yellow curve) one-dimensional scattering patterns from the fullerene-C60 powder sample in different experimental conditions in SANS and WANS geometries, as explained in the legends, in parallel with the XRD pattern (green curve). For better comparison, the XRD data were normalized to the SANS peak intensity and elevated so that the baseline corresponds to the flat SANS background.

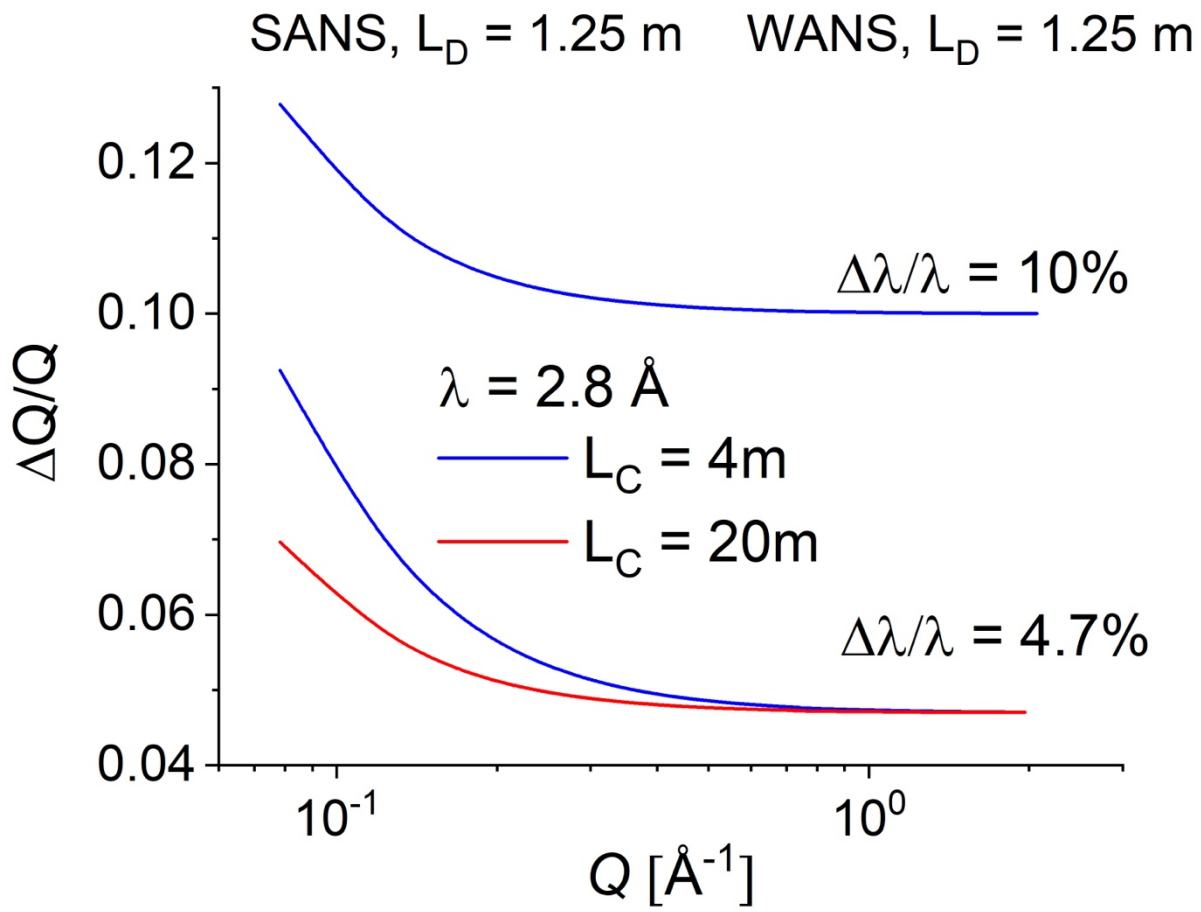

Figure 6 The *Q*-resolution at KWS-2 for the SANS and WANS detectors under different experimental conditions (L_D, L_C, λ and Δλ).